CHARACTERIZING SPECTRAL DIVERSITY IN CARBONACEOUS CHONDRITES AND LINKING METEORITES TO ASTEROIDS WITH MICROIMAGING SPECTROSCOPY. S. A. Parra[1], B. L. Ehlmann[1,2], M. Velbel[3,4], [1]Div. of Geological & Planetary Sciences, California Institute of Technology, Pasadena, CA (sparra@caltech.edu), [2]Jet Propulsion Laboratory, California Institute of Technology, Pasadena, CA. [3]Michigan State University, Lansing, MI. [4]Smithsonian Institution, Washington, DC.

Introduction: Primitive asteroids record processes active in the early Solar System, [1, 2]. Telescopic visible and shortwave infrared (VSWIR) spectroscopy of primitive asteroids has led to definition of broad spectral classes generally indicative of differentiation and alteration processes [1, 3]. However, these spatially unresolved observations hinder tying specific, observed spectral feature differences to particular phases, petrologic contexts, and alteration histories.

Microimaging VSWIR reflectance spectroscopy of carbonaceous chondrites – meteorites originating from primitive asteroids – provides µm-scale records of formation and alteration processes undergone by their parent bodies [2, 4]. Microimaging spectroscopy enables rapid and non-destructive spectral mapping of chondrites [5], improving upon previous bulk powder observations by preserving petrologic textures and spatial heterogeneity in spectral properties. Spectral mapping thus enables a more precise identification of the compositional drivers behind the spectral features observed [3]. We thus aim to characterize the observed spectral diversity in a suite of carbonaceous chondrites, and link these to the spectral diversity observed in primitive asteroids and the phases responsible.

Methods: We collected spectral image cubes for samples from 19 carbonaceous chondrites over a range of petrologic types (Table 1) with the Ultra-Compact Imaging Spectrometer (UCIS) at the Jet Propulsion Laboratory. UCIS observes the 0.4-2.6 µm wavelength range at a ~80 µm/pixel spatial resolution [6]. Data were measured with 20 ms integration times and calibrated to absolute reflectance with a 20% Spectralon target. We then applied an adaptive Savitzky-Golay smoothing filter to reduce noise and performed principal component analysis (PCA) on the image cubes using an adapted processing pipeline and eigenvectors from [7] to observe the chondrites along key axes of dataset variance derived from the classified asteroids. The data were down-sampled to 41 channels for PCA, but all other analyses were done at native (206 channel) resolution. We also obtained bulk spectra by averaging over the area covered by each meteorite and transformed them via PCA.

Table 1. The carbonaceous chondrites imaged for this study.

Type	Sample Name
CM1	Moapa Valley, SCO 06043
CM1/2	ALH 83100
CM2	ALH 83102, ALH 84044, LEW 90500, LON 94101, MET 00639, Murchison
CM anomalous	WIS 91600, PCA 91008
CR2	NWA 7502
CV3	Allende, Leoville, NWA 3118, NWA 4446
C2, ungrouped	Tagish Lake
C1	Y-82162, Y-980115

PCA & Comparison to Asteroids: PC 1 and PC 3 show the greatest separation of the chondrites, which [7] observed separated asteroids based on absorptions at ~2 µm and ~1 µm, respectively. The chondrites cluster apart from the S-class and group with the X, D, and C-classes (Fig. 1). Interestingly, they group closer with the X class rather than the C-class asteroids, which are thought to be the carbonaceous chondrite parent bodies. This may be driven by chondrules with 1- and 2-µm mafic features at this spatial scale. The density cloud in Fig. 1 shows the highest density of pixels within the range of the bulk spectra, although lobes extending from the cloud reveal spectral endmembers.

Endmember Analysis: We examined spectra of endmember A and B lobes in the Fig. 1 density cloud (Fig. 2). Endmember A corresponds to olivine, which in CR2 chondrites has been observed in both chondrules and in the matrix [8] (Fig. 2b). Both the sample and mean spectra for A also feature shallow absorptions at 1.9 and ~2.3-µm, which indicate alteration of olivine at the sub-pixel scale. Endmember B, by contrast, corresponds with Fe-oxidation products, marked by ferric iron absorptions at 0.8-0.9 µm and a shallow hydration feature at 1.9 µm. In our dataset, we primarily observe these in CR2 chondrites. The distribution of Endmember B also agrees with literature on the dominance of terrestrial weathering products such as

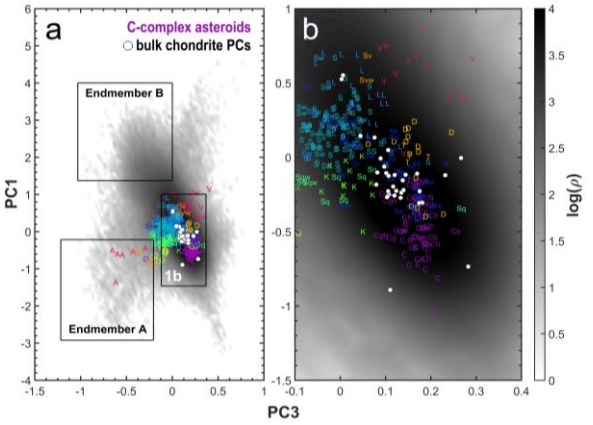

Figure 1. a) The first and third principal components of the asteroid eigenspace, where a density cloud reveals the spread of individual chondrite image pixels compared to the bulk averages (white circles) and asteroid spectral classes, including the C-complex asteroids (purple). Endmembers A and B are boxed in black; b) a zoomed-in view of a) with the distribution of the bulk chondrite PCs.

Fe-oxides/oxyhydroxides on CR2 bulk spectra, which complicates determining the initial degree of aqueous alteration on the parent body [8].

Fe-serpentine Alteration: Key features reported for CM chondrites include absorptions around 0.7, 0.9 and 1.1 μm, attributed to Fe (II)/Fe (III) in serpentine-group phyllosilicates, which partly originate from olivine alteration [9]. We observe these features in some bulk CM spectra of our samples (Fig. 3a). In initial mapping of absorption spatial distributions, we compared them to locations bearing olivine-like features. In CM chondrites, olivine is mostly limited to chondrules and other lithic fragments, as the matrix is dominated by phyllosilicates [9]. Only a few sample regions (3f, point Z) have clearly identified Fe-serpentine-like absorptions, however. The low signal-to-noise ratio in the matrix data of this sample means the majority of spectra with the serpentine absorptions are associated with chondrules and lithic fragments. A preliminary comparison to RELAB-documented clays reveals a closer similarity to the chlorite-group Fe-endmember chamosite than cronstedtite, however. This may support observations of chlorite as an intermediate alteration product of olivine in CM chondrites [9].

Future Work: Further work will focus on semi-automated extraction of spectral endmembers at native spectral resolution, including in the dark matrix. We will utilize other absorptions to identify serpentine and chlorite minerals, such as the OH vibrational modes at 1.4-μm and metal-OH vibrational modes near 2.3-μm.

Acknowledgments: Thanks to F. DeMeo for help with providing asteroid pipeline information. This work was funded by a NASA Emerging Worlds grant to B.L.E. (#80NSSC18K0593).

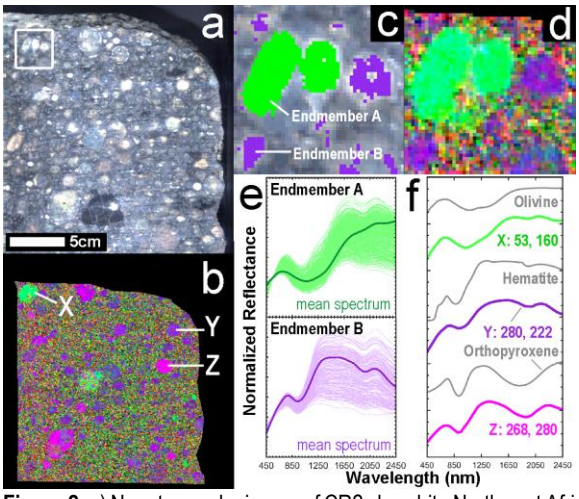

Figure 2. a) Near true-color image of CR2 chondrite Northwest Africa 7502 (NWA 7502); b) RGB parameter map with key absorptions for low-Ca pyroxene (R: band depth (BD) at 1.9 μm), olivine (G: OLINDEX – based on reflectances at 1.05, 1.21, 1.33, 1.47, and 1.695 μm), and ferric iron (B: BD at 0.92 μm); c) ROIs for pixels within each endmember lobe; d) a zoomed-in view of b); e) lighter spectra correspond to the member pixels shown in c) with mean spectrum in bold; f) sample spectra from b) with RELAB spectra for olivine, hematite, and orthopyroxene.

References: [1] DeMeo, F. E., & Carry, B. (2014) *Nature*, 505(7485), 629–634. [2] Johansen, A., et al., (2015) *Science Adv., 1*(3), e1500109. [3] Takir, D., & Emery, J. P. (2012) *Icarus*, *219*(2), 641–654. [4] Scott, E. R. (2007) *Ann. Rev. of Earth & Plan. Sci., 35*(1), 577–620. [5] Greenberger, R. N., et al., (2015) *GSA Today*, *25*(12), 4–10. [6] Van Gorp, B., et al., (2014) *J. of App. Rem. Sens.*, *8*(1), 084988. [7] DeMeo, et al., (2009) *Icarus*, *202*(1), 160–180. [8] Cloutis et al., (2011) *Icarus*, 216(1), 309-46. [9] Cloutis et al., (2012) *Icarus*, 217(1), 389-407.

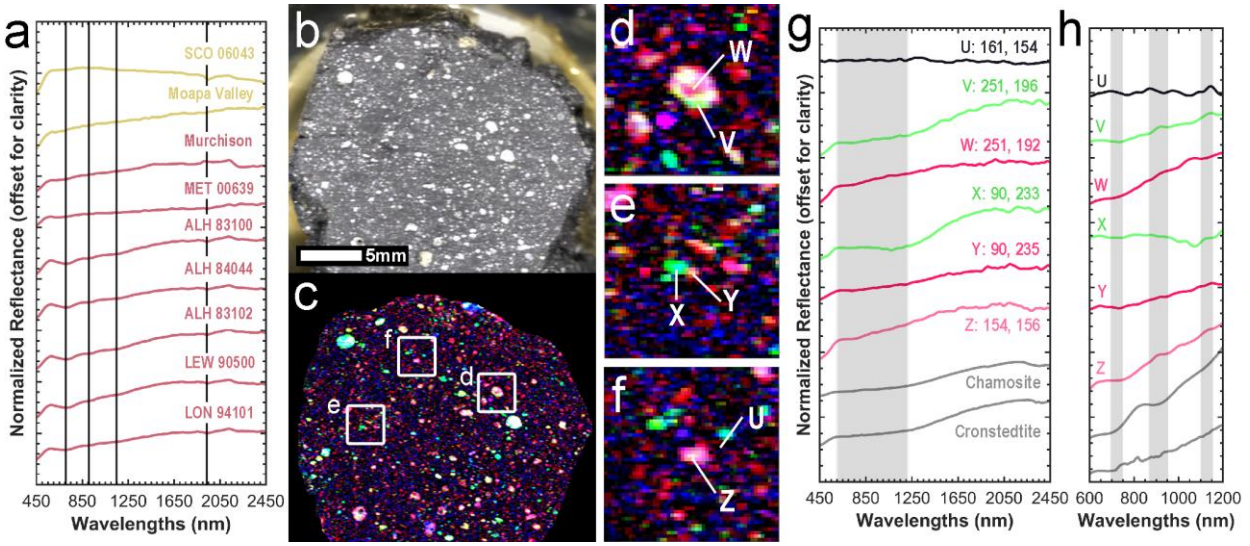

Figure 3. a) Bulk-averaged spectra for the CM chondrites used in the study, where lines at 0.7, 0.9, and 1.1um indicate observed absorption features; b) near-true color image of CM2 chondrite Murchison; c) RGB parameter map of Murchison, showing the presence of alteration features at 900nm (R: BD900) and 1100nm (B: BD1100) compared to olivine (G: OLINDEX); d-f) zoomed-in views of c) indicating contrasts between olivine and the alteration signatures; g) sample spectra from d-f) with the spectra range for the alteration features (gray) alongside RELAB spectra for chamosite and cronstedtite; h) a zoomed-in view of g, highlighting the spectral range for each of the absorption features previously observed for CM chondrites compared to the features for chamosite and cronstedtite